Investigation of the numerics of point spread function integration in single molecule localization

Jerry Chao,[1,2,6] **Sripad Ram,**[3,5,6] **Taiyoon Lee,**[3] **E. Sally Ward,**[2,4] **and Raimund J. Ober**[1,2,*]

[1]*Department of Biomedical Engineering, Texas A&M University, College Station, TX 77843, USA*
[2]*Department of Molecular and Cellular Medicine, Texas A&M Health Science Center, College Station, TX 77843, USA*
[3]*Department of Electrical Engineering, University of Texas at Dallas, Richardson, TX 75080, USA*
[4]*Department of Microbial Pathogenesis and Immunology, Texas A&M Health Science Center, College Station, TX 77843, USA*
[5]*Present address: Carl Zeiss Microscopy, One Zeiss Drive, Thornwood, NY 10594, USA*
[6]*These authors contributed equally to this work.*
[*]*raimund.ober@tamu.edu*

Abstract: The computation of point spread functions, which are typically used to model the image profile of a single molecule, represents a central task in the analysis of single molecule microscopy data. To determine how the accuracy of the computation affects how well a single molecule can be localized, we investigate how the fineness with which the point spread function is integrated over an image pixel impacts the performance of the maximum likelihood location estimator. We consider both the Airy and the two-dimensional Gaussian point spread functions. Our results show that the point spread function needs to be adequately integrated over a pixel to ensure that the estimator closely recovers the true location of the single molecule with an accuracy that is comparable to the best possible accuracy as determined using the Fisher information formalism. Importantly, if integration with an insufficiently fine step size is carried out, the resulting estimates can be significantly different from the true location, particularly when the image data is acquired at relatively low magnifications. We also present a methodology for determining an adequate step size for integrating the point spread function.

OCIS codes: (180.2520) Fluorescence microscopy; (110.3055) Information theoretical analysis; (100.2960) Image analysis; (000.5490) Probability theory, stochastic processes, and statistics.

References and links

1. R. J. Ober, S. Ram, and E. S. Ward, "Localization accuracy in single-molecule microscopy," Biophys. J. **86**(2), 1185–1200 (2004).
2. W. E. Moerner, "New directions in single-molecule imaging and analysis," Proc. Natl. Acad. Sci. USA **104**(31), 12596–12602 (2007).
3. E. Betzig, G. H. Patterson, R. Sougrat, O. W. Lindwasser, S. Olenych, J. S. Bonifacino, M. W. Davidson, J. Lippincott-Schwartz, and H. F. Hess, "Imaging intracellular fluorescent proteins at nanometer resolution," Science **313**(5793), 1642–1645 (2006).

#237601 Received 6 Apr 2015; revised 18 May 2015; accepted 28 May 2015; published 18 Jun 2015

4. M. J. Rust, M. Bates, and X. Zhuang, "Sub-diffraction-limit imaging by stochastic optical reconstruction microscopy (STORM)," Nat. Methods **3**(10), 793–795 (2006).
5. S. T. Hess, T. P. K. Girirajan, and M. D. Mason, "Ultra-high resolution imaging by fluorescence photoactivation localization microscopy," Biophys. J. **91**(11), 4258–4272 (2006).
6. M. Born and E. Wolf, *Principles of Optics* (Cambridge University, 1999).
7. U. Kubitscheck, O. Kückmann, T. Kues, and R. Peters, "Imaging and tracking of single GFP molecules in solution," Biophys. J. **78**(4), 2170–2179 (2000).
8. M. K. Cheezum, W. F. Walker, and W. H. Guilford, "Quantitative comparison of algorithms for tracking single fluorescent particles," Biophys. J. **81**(4), 2378–2388 (2001).
9. R. E. Thompson, D. R. Larson, and W. W. Webb, "Precise nanometer localization analysis for individual fluorescent probes," Biophys. J. **82**(5), 2775–2783 (2002).
10. I. J. Cooper and C. J. R. Sheppard, "A matrix method for calculating the three-dimensional irradiance distribution in the focal region of a convergent beam," Optik **114**(7), 298–304 (2003).
11. J. Markham and J.-A. Conchello, "Numerical evaluation of Hankel transforms for oscillating functions," J. Opt. Soc. Am. A **20**(4), 621–630 (2003).
12. C. S. Smith, N. Joseph, B. Rieger, and K. A. Lidke, "Fast, single-molecule localization that achieves theoretically minimum uncertainty," Nat. Methods **7**(5), 373–375 (2010).
13. A. Sergé, N. Bertaux, H. Rigneault, and D. Marguet, "Dynamic multiple-target tracing to probe spatiotemporal cartography of cell membranes," Nat. Methods **5**(8), 687–694 (2008).
14. A. V. Abraham, S. Ram, J. Chao, E. S. Ward, and R. J. Ober, "Quantitative study of single molecule location estimation techniques," Opt. Express **17**(26), 23352–23373 (2009).
15. S. Ram, E. S. Ward, and R. J. Ober, "A novel resolution measure for optical microscopes: stochastic analysis of the performance limits," in Proceedings of the 3rd IEEE International Symposium on Biomedical Imaging: Nano to Macro (IEEE, 2006), pp. 770–773.
16. S. Ram, E. S. Ward, and R. J. Ober, "A stochastic analysis of performance limits for optical microscopes," Multidim. Syst. Sign. P. **17**(1), 27–57 (2006).
17. P. J. Huber and E. M. Ronchetti, *Robust Statistics*, 2nd ed. (Wiley, 2009).
18. C. R. Rao, *Linear Statistical Inference and its Applications* (Wiley, 1965).
19. J. Chao, E. S. Ward, and R. J. Ober, "Fisher information matrix for branching processes with application to electron-multiplying charge-coupled devices," Multidim. Syst. Sign. P. **23**(3), 349–379 (2012).
20. T. Sauer, *Numerical Analysis* (Pearson, 2005).

1. Introduction

In single molecule microscopy, accurately determining the location of a single molecule is a central problem that has significant implications for the analysis of the acquired data [1, 2]. For instance, in localization microscopy the accuracy with which the position of a single molecule can be estimated influences the resolution of the reconstructed superresolution image, which in turn affects the interpretation of the results [3–5]. The localization algorithm typically consists of a curve fitting procedure wherein an appropriately chosen parametric image profile is fitted to a region of interest in the image to determine the position of the single molecule. The selected image profile is typically assumed to model the point spread function of the microscope. According to optical diffraction theory, the image of a point-like object such as a single molecule is given by a diffraction integral [6]. In the special case when the point source is in focus, the diffraction integral reduces to the well-known Airy profile which has a closed-form analytical expression. In many single molecule imaging applications, various research groups assume a two-dimensional (2D) Gaussian profile to model the point spread function of the microscope [7–9].

An important aspect of single molecule localization and, more generally, of any parametric estimation procedure, is the numerical computation of the image profile that is used in the curve-fitting procedure. It is recognized that appropriate numerical evaluation of the point spread function is important for the proper representation of the image profile [10, 11]. The image of a single molecule at the detector plane is a continuous image profile. However, due to the presence of pixels in the imaging detector, the image that is captured by the detector is a sampled version of this continuous image, such that the detected intensity at each pixel is an integral of the continuous image over that pixel. While some groups have modeled the pixelated

#237601 Received 6 Apr 2015; revised 18 May 2015; accepted 28 May 2015; published 18 Jun 2015

image of a single molecule by accurately computing the integral over each pixel [1, 4, 12], others have chosen to use a simple integration method that evaluates the continuous image at only one point over each pixel [13]. The question thus arises as to how the fineness of integration over a pixel, in other words the number of points on the pixel at which the image profile is evaluated, affects the performance of the location estimator. This question is also of relevance from a computational standpoint, in that fewer evaluations of the image profile could lead to much faster code execution, but at the possible expense of estimator performance.

In this paper, we address the above question by investigating the behavior of the maximum likelihood (ML) estimator, which has been shown to have favorable properties in the context of single molecule localization [1, 12, 14]. We consider the in-focus scenario and fit the Airy and the 2D Gaussian profile to simulated single molecule images. For both image profiles, we consider four imaging scenarios with different levels of signal and additive noise sources. In addition, we look at two different magnifications, which importantly yield different samplings of a given image profile, and hence are expected to affect the fineness with which the ML estimator needs to integrate the image profile over the pixels. We evaluate the performance of the ML estimator by calculating the median and accuracy (i.e., standard deviation with respect to the median) of the location estimates, and comparing them, respectively, to the true positional coordinates of the single molecule and the Fisher information-based limit of the localization accuracy, which gives the best possible standard deviation with which the coordinates can be determined.

Note that for the evaluation of the 2D Gaussian profile over a pixel, an analytical alternative to numerical integration is an implementation that uses the error function [4, 12, 15], which is both accurate and fast. We nevertheless choose to consider the 2D Gaussian profile in the current study, so that we have two different and commonly used image profiles with which to investigate the effect of the fineness of integration.

The remainder of this paper is organized as follows. In Section 2, we provide a description of the single molecule image data model, which forms the basis for the simulation of the image data, the derivation of the likelihood function that is maximized by the ML estimator, and the calculation of the Fisher information-based accuracy benchmark against which the standard deviation of a given set of location estimates is compared. In Section 3, we describe the ML estimator, and define quantities that are used to assess its performance. In Section 4, we detail the settings for which the image data sets analyzed in this paper are simulated. In Section 5, we define and illustrate a quantity which we use to specify the fineness of integration over an image pixel, and which we employ in the subsequent interpretation of our results. In Section 6, we present and discuss the results of the ML estimations carried out on our simulated data, and propose a methodology for obtaining a guideline for determining an appropriate fineness of integration. Lastly, we conclude in Section 7.

2. Single molecule image model

The image of a single molecule that is acquired by a pixelated detector is given by [1, 16]

$$I_{\theta,k} = S_{\theta,k} + B_k + W_k, \quad k = 1, \ldots, K_{pix}, \quad \theta \in \Theta, \tag{1}$$

where K_{pix} denotes the total number of pixels in the single molecule image, θ denotes the unknown parameter vector that we wish to estimate, and Θ denotes the parameter space. The term $S_{\theta,k}$ is a Poisson random variable with mean $\mu_{\theta,k}$ that represents the number of photons detected at the kth pixel from the single molecule. The term B_k is a Poisson random variable with mean b_k that represents the number of background photons detected at the kth pixel. The term W_k is a Gaussian random variable with mean η_k and variance $\sigma^2_{w,k}$ that represents the measurement noise (i.e., the detector's readout noise) at the kth pixel. The three random variables are

#237601 Received 6 Apr 2015; revised 18 May 2015; accepted 28 May 2015; published 18 Jun 2015

mutually independent of one another. The mean $\mu_{\theta,k}$ of $S_{\theta,k}$ is given by

$$\mu_{\theta,k} = \frac{N}{M^2}\int_{C_k} q_{z_0}\left(\frac{x}{M}-x_0,\frac{y}{M}-y_0\right)dxdy, \quad \theta\in\Theta, \tag{2}$$

where N denotes the average number of photons detected at the detector plane from the single molecule, M denotes the lateral magnification of the imaging system, (x_0,y_0,z_0) denotes the three-dimensional location of the single molecule in the object space, and C_k denotes the region on the detector plane occupied by the kth pixel, $k=1,\ldots,K_{pix}$. The function q_{z_0} is referred to as the image function [16], and it describes the image, captured at unit magnification, of a point source that is located along the optical axis at position z_0. In this paper, we consider the case where the single molecule is in focus (i.e., $z_0=0$), and has an image described by either the Airy profile or the 2D Gaussian profile, with image function given by

$$q_{z_0}(x,y) = q(x,y) = \frac{J_1^2(\alpha\sqrt{x^2+y^2})}{\pi(x^2+y^2)}, \quad (x,y)\in\mathbb{R}^2, \quad \text{(Airy profile)} \tag{3}$$

$$q_{z_0}(x,y) = q(x,y) = \frac{1}{2\pi\sigma^2}\cdot e^{-\frac{x^2+y^2}{2\sigma^2}}, \quad (x,y)\in\mathbb{R}^2. \quad \text{(2D Gaussian profile)} \tag{4}$$

In the equation for the Airy profile, $\alpha = 2\pi n_a/\lambda$, where n_a denotes the numerical aperture of the objective lens and λ denotes the wavelength of the detected photons. In the equation for the 2D Gaussian profile, σ^2 is the variance of the Gaussian function.

3. Maximum likelihood estimator

The maximum likelihood (ML) estimator is a specific algorithm that estimates an unknown parameter vector θ by maximizing the likelihood function of the underlying data with respect to θ. The likelihood function $\mathscr{L}$ for the image of a single molecule that is acquired with a pixelated detector is given by [1, 16]

$$\mathscr{L}(\theta \mid z_1,\ldots,z_{K_{pix}}) = \prod_{k=1}^{K_{pix}} p_{\theta,k}(z_k), \quad \theta\in\Theta, \tag{5}$$

where $\{z_1,\ldots,z_{k_{pix}}\}$ denotes the acquired data and $p_{\theta,k}$ denotes the probability distribution function of the data acquired at the kth pixel. The probability distribution function depends on the point spread function, via the image profile q in the expression for the mean photon count detected at the pixel from the single molecule (i.e., Eq. (2)). Its analytical expression also depends on the presence and types of additive noise sources, and is given in Appendix A.1.

The ML estimate of θ is determined by maximizing the logarithm of the likelihood function, and is given by

$$\hat{\theta}_{ML} = \text{argmax}_\theta\left(\sum_{k=1}^{K_{pix}}\log(p_{\theta,k}(z_k))\right). \tag{6}$$

All computations were carried out in the MATLAB (The MathWorks, Inc., Natick, MA) programming language, and the ML estimator was implemented using the *fminunc* function of the MATLAB optimization toolbox. The parameters x_0 and y_0 were floated during the estimation procedure (i.e., $\theta=(x_0,y_0)$), while the width parameter of the image profile (α for the Airy profile and σ for the 2D Gaussian profile), the average single molecule photon count N, and the average background photon count b_k at the kth pixel, $k=1,\ldots,K_{pix}$, were fixed to their respective true values. In the practical context, the fixing of the values of the width, photon count, and

#237601 Received 6 Apr 2015; revised 18 May 2015; accepted 28 May 2015; published 18 Jun 2015

background photon count parameters implies that they have first been independently estimated, which can typically be done.

During the maximization, the point spread function is repeatedly computed via Eq. (2) as the ML estimator tries different values of x_0 and y_0. It is the evaluation of the integral of the image profile q over the pixel region C_k in Eq. (2) that is investigated in this paper.

3.1. Quantifying the performance of the ML estimator

In this paper, we use the ML estimator to determine the location of a single molecule from simulated image data. To assess the estimator's performance, we look at both its ability to closely recover the true location of the molecule, and the accuracy with which it can do so. To evaluate the former, often the mean of the estimated locations is calculated and compared with the true value. However, especially in cases where the image data is characterized by relatively low signal levels from the molecule and relatively high noise levels (e.g., data scenario 4; see Section 4), we have had evidence of outliers as estimates, which were probably due to the estimator's convergence to local minima. In order for our analysis to not be unduly influenced by outliers, we look instead at the median of the estimates, as the median is known to be more robust than the mean to the effect of potential outlying estimates [17].

We therefore compute the median, as well as the standard deviation with respect to the median, of the estimated positional coordinates, and quantify their closeness to the true value and the best possible standard deviation, respectively, via a simple difference d and a percentage difference δ, which we describe here.

For use in assessing the performance of the ML estimator in terms of its ability to recover the true location of the single molecule, we compute the difference d between the median of the estimates and the corresponding true value. For example, for the x_0 coordinate, the difference is given by

$$d(x_0) = \text{median}(\hat{x}_0) - x_0, \tag{7}$$

where $\hat{x}_0$ denotes the ML estimate of x_0.

For use in assessing the performance of the ML estimator in terms of its accuracy, we make use of the Fisher information matrix which, through the Cramér-Rao inequality [18], provides a limit to the accuracy (i.e., the best possible accuracy) with which an unknown parameter can be determined. By definition, the Fisher information matrix is independent of the estimation algorithm and only depends on the statistical description of the acquired data.

The general expression for the Fisher information matrix for an image acquired with a pixelated detector is given by [16, 19]

$$\mathbf{I}(\theta) = \sum_{k=1}^{K_{pix}} \frac{\kappa_{\theta,k}}{\nu_{\theta,k}} \left(\frac{\partial \mu_{\theta,k}}{\partial \theta} \right)^T \frac{\partial \mu_{\theta,k}}{\partial \theta}, \quad \theta \in \Theta, \tag{8}$$

where $\kappa_{\theta,k}$ denotes the noise coefficient for the kth pixel, and $\nu_{\theta,k} = \mu_{\theta,k} + b_k$, with $\mu_{\theta,k}$ as given by Eq. (2) and b_k the average number of background photons at the kth pixel as defined in Section 2. The analytical expression for the noise coefficient $\kappa_{\theta,k}$ depends on the presence and types of additive noise sources, and can be found in Appendix A.2.

Given the Fisher information matrix $\mathbf{I}(\theta)$, where the unknown parameter vector $\theta = (x_0, y_0)$, the best possible standard deviation with which the positional coordinate x_0 can be estimated is given by $\sqrt{[\mathbf{I}^{-1}(\theta)]_{11}}$, as per the Cramér-Rao inequality. The subscript 11 denotes element $(1,1)$, or the first main diagonal element, of the inverse Fisher information matrix, which corresponds to the parameter x_0. Similarly, the best possible standard deviation with which y_0 can be estimated is given by $\sqrt{[\mathbf{I}^{-1}(\theta)]_{22}}$. Using previously defined terminology [14], we refer to these best possible standard deviations as the practical localization accuracy measure (PLAM) for x_0 and y_0, and denote them by $\text{PLAM}(x_0)$ and $\text{PLAM}(y_0)$.

#237601 Received 6 Apr 2015; revised 18 May 2015; accepted 28 May 2015; published 18 Jun 2015

Table 1. Signal and additive noise levels for the four data scenarios considered

Scenario	Mean number of single molecule photons N	Mean number of background photons per pixel	Mean of readout noise (e^-/pixel)	Std. dev. of readout noise (e^-/pixel)
1	3000	0	0	0
2	3000	50	0	2
3	300	0	0	0
4	300	100	0	6

We quantify the closeness of the standard deviation of the obtained estimates to the PLAM by the percentage difference δ between the two numbers. For example, for the x_0 coordinate, the percentage difference $\delta(x_0)$ is given by

$$\delta(x_0) = \frac{\mathrm{sd}(\hat{x}_0) - \mathrm{PLAM}(x_0)}{\mathrm{PLAM}(x_0)} \times 100, \tag{9}$$

where sd denotes the standard deviation.

From the definitions of Eqs. (7) and (9), it follows that for an ideal estimator that recovers the true value and attains the PLAM, the difference d and the percentage difference δ will be zero.

4. Simulated data sets

Single molecule images were generated according to the image model of Eq. (1), using the *poissrnd* function of the MATLAB statistics toolbox for the generation of Poisson random variables, and the *randn* function of MATLAB for the generation of Gaussian random variables. We simulated data under four scenarios that differ in terms of signal and additive noise levels, the details of which are presented in Table 1. Note that in scenarios 2 and 4, where additive noise sources are present, photons due to the background component are assumed to be uniformly distributed throughout the image, such that the mean number of background photons is the same at each image pixel. Similarly, the readout noise is assumed to be statistically identical for each image pixel (i.e., its mean and standard deviation are the same for every pixel).

A given data set comprises 1000 repeat images of a single molecule, simulated under the conditions of one of the four scenarios. In all simulations, the image array size is set to 11×11 pixels, the lateral magnification is set to $M = 100$ or $M = 63$, each representing a common magnification for objective lenses used in single molecule microscopy (see, e.g., [7, 13]), the numerical aperture is set to $n_a = 1.4$, the wavelength of the detected photons is set to $\lambda = 669$ nm, the pixel size is set to $16\,\mu\mathrm{m} \times 16\,\mu\mathrm{m}$, and the positional coordinates of the single molecule are set to $(x_0, y_0) = (848\ \mathrm{nm}, 816\ \mathrm{nm})$ for $M = 100$, and $(x_0, y_0) = (1346.03\ \mathrm{nm}, 1295.24\ \mathrm{nm})$ for $M = 63$, in each case placing the molecule at 5.3 pixels in the x direction and 5.1 pixels in the y direction within the image array. The images were simulated using either an Airy profile or a 2D Gaussian profile. For the Gaussian profile, the width (i.e., standard deviation) of the Gaussian function is set to $\sigma = 100.62$ nm. For the ML estimation, images simulated with an Airy profile were fitted with an Airy profile, and images simulated with a 2D Gaussian profile were fitted with a 2D Gaussian profile.

5. Investigating the impact of the fineness of image profile integration

The purpose of this paper is to investigate how the fineness of the integration of the image profile over a pixel impacts the performance of the ML location estimator. Specifically, we

#237601 Received 6 Apr 2015; revised 18 May 2015; accepted 28 May 2015; published 18 Jun 2015

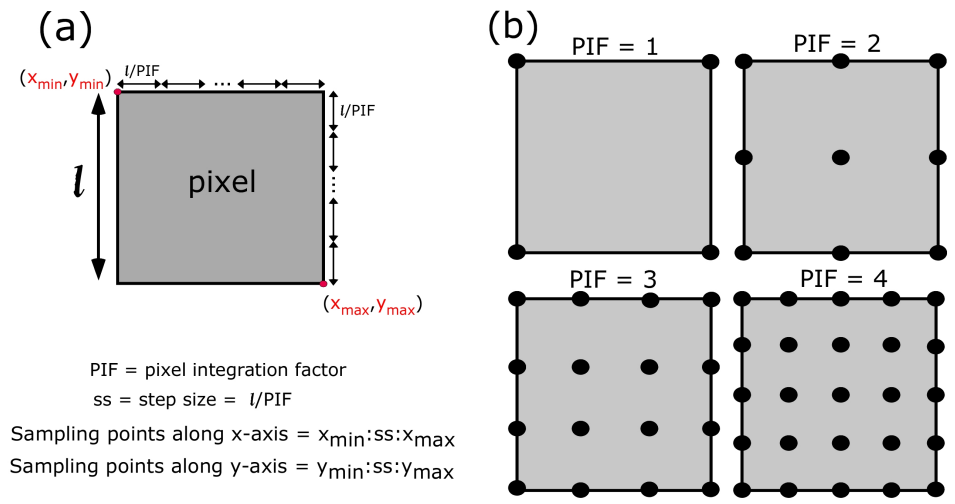

Fig. 1. Fineness of integration of the image profile. (a) Sampling scheme for the 2D trapezoidal method of integration over a square pixel with side length l. The integration step size ss is defined as l divided by the pixel integration factor (PIF). The notation $x_{min} : ss : x_{max}$ denotes the positions $\{x_{min},\ x_{min}+ss,\ x_{min}+2\cdot ss,\ \ldots,\ x_{max}\}$ along the x-axis at which the image profile is evaluated, and the notation $y_{min} : ss : y_{max}$ denotes analogous positions along the y-axis. (b) Examples showing the location of the sampling points within a pixel for different values of the PIF. A PIF value of n, where $n = 1,2,\ldots$, means that the image profile is evaluated at $(n+1)^2$ evenly spaced points covering the pixel area.

consider the 2D trapezoidal method of numerical integration [20], and we study how changing the step size used in the integration of the image profile q in Eq. (2) impacts the estimation of the single molecule's positional coordinates x_0 and y_0. Given the square pixel assumed in this paper (which is typical of the cameras used in single molecule microscopy), we specify the integration step size in terms of a number we refer to as the pixel integration factor (PIF). For a square pixel with side length l, the step size is just l/PIF in both the x and y directions, so that a PIF value of n, where $n = 1,2,\ldots$, means that the pixel will be sampled at $(n+1)^2$ evenly spaced points covering its area. The sampling scheme is illustrated in Fig. 1(a), and examples for four different PIF values are shown in Fig. 1(b).

Importantly, a PIF value of 0 specifies the simple integration method in which the mean single molecule photon count at each pixel is computed by taking the value of the image profile q at the center of the pixel and multiplying it by the area of the pixel. For each pixel, this method of integration requires the evaluation of the image profile at only a single point, and approximates the volume under the profile and over the pixel by the volume of the rectangular box having the pixel as its base and the profile's value at the center of the pixel as its height.

For our investigation, the simulated image data described in Section 4 was generated using a PIF value of 13, the largest PIF value considered in this paper. Each data set was then subjected to ML estimation where the repeated computation of the image profile q was done using PIF values ranging from 0 to 13. In accordance with the integration step size used in the data simulation, the PLAM (see Section 3.1), against which the standard deviation of a given set of location estimates is compared, was also calculated using a PIF value of 13.

Note that other numerical integration methods [20] and sampling schemes can also be used to integrate image profiles over pixels, and that in principle, they can be used to perform the

#237601 Received 6 Apr 2015; revised 18 May 2015; accepted 28 May 2015; published 18 Jun 2015

same type of study.

6. Results

Figure 2 shows the results of ML estimations carried out on the data sets simulated with the Airy image profile, according to the four scenarios of Table 1 and the descriptions in Section 4. Figure 3 analogously shows the results for the data sets simulated with the 2D Gaussian image profile. In each figure, both the difference d between the median of the estimates and the true value, and the percentage difference δ between the standard deviation of the estimates and the PLAM, are plotted as a function of the PIF used by the ML estimator. In all cases, the quantities d and δ are calculated based on the median and standard deviation of the 1000 estimates obtained from the 1000 images comprising the data set. Only the results for the x_0 coordinate are shown, as the results for the y_0 coordinate are similar. Note also that for each data set presented in Figs. 2 and 3, we also analyzed two additional statistically identical data sets, and found the results to agree well with the results discussed here.

6.1. Proper integration of the image profile

We first examine the results for PIF = 13, which we take to be the reference results because PIF = 13 was used to simulate the data on which the ML estimations were carried out. For all four scenarios and both the 100× and 63× magnifications, the plots of Figs. 2 and 3 show that the difference d is close to zero at PIF = 13, suggesting that the ML estimator can closely recover the true value x_0. For all four scenarios and both magnifications, the magnitude of d at PIF = 13 is no greater than 0.21 nm (magnitude of d for scenario 3, 100× magnification) in Fig. 2, and 0.72 nm (magnitude of d for scenario 3, 100× magnification) in Fig. 3.

In terms of the accuracy, the percentage difference δ at PIF = 13 is below 4%, for both magnifications, in scenarios 1, 2, and 3 in both Figs. 2 and 3. The small percentages indicate that when the signal level N from the single molecule is large in comparison to noise from both the background component and the camera's readout process, the accuracy of the ML estimator can be expected to be comparable to the PLAM. On the other hand, in the case of scenario 4 where the signal level is not large compared to the noise levels, δ at PIF = 13 can be relatively big, suggesting that the accuracy of the estimator may not be as close to the PLAM under such conditions. In our examples this is particularly the case for the 63× magnification, where the magnitude of δ at PIF = 13 is 19% for the Airy profile data set, and 12% for the 2D Gaussian profile data set.

6.2. Simple integration of the image profile

We next consider the results for PIF = 0, where instead of using the 2D trapezoidal method to integrate the image profile over a given pixel, the ML estimator integrates the profile by multiplying the profile's value at the center of the pixel by the area of the pixel. In terms of the ability of the estimator to recover the true value x_0, the plots of Figs. 2 and 3 demonstrate that this simple method of profile integration can sometimes lead to a difference d that is substantially larger (i.e., worse) than d at PIF = 13. This is true for the 63× magnification example, where in each of the four scenarios, the magnitude of d at PIF = 0 is greater than 30 nm in Fig. 2 and 17 nm in Fig. 3.

For the 100× magnification, d at PIF = 0 is not nearly as large, but in most cases still non-trivially bigger than d at PIF = 13. For each of the four 100× Airy profile data sets of Fig. 2, for example, the magnitude of d at PIF = 0 is no smaller than 1.5 nm, which is significant compared to the aforementioned largest d magnitude of 0.21 nm at PIF = 13. Our results do suggest, however, that in certain cases d at PIF = 0 can be very comparable to d at PIF = 13. For example, for the 100× 2D Gaussian profile data sets of scenarios 1, 2, and 3 in Fig. 3, the values

#237601 Received 6 Apr 2015; revised 18 May 2015; accepted 28 May 2015; published 18 Jun 2015

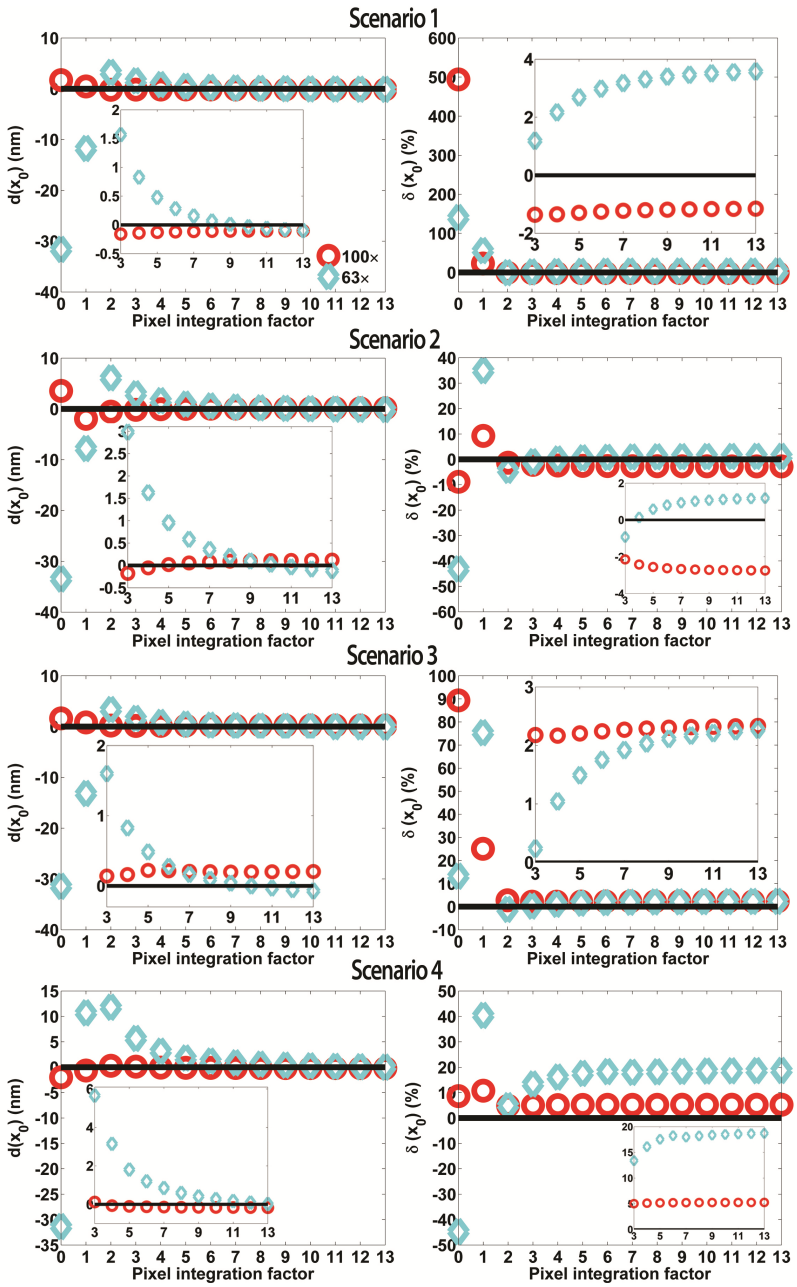

Fig. 2. Airy profile results: difference $d(x_0)$ between the median of the x_0 estimates and the true value x_0 (left-hand side plots), and percentage difference $\delta(x_0)$ between the standard deviation (with respect to the median) of the x_0 estimates and the PLAM for x_0 (right-hand side plots), as functions of the PIF used to integrate the image profile during estimation. For each scenario of Table 1, results are shown for a 63× (cyan ⋄) and a 100× (red ○) data set, simulated at PIF = 13 using the Airy profile with parameters given in Section 4. Each data set is fitted with an Airy profile by an ML estimator, with PIF values ranging from 0 to 13. In all plots the horizontal line denotes 0, and the inset shows the results for PIF ≥ 3.

#237601 Received 6 Apr 2015; revised 18 May 2015; accepted 28 May 2015; published 18 Jun 2015

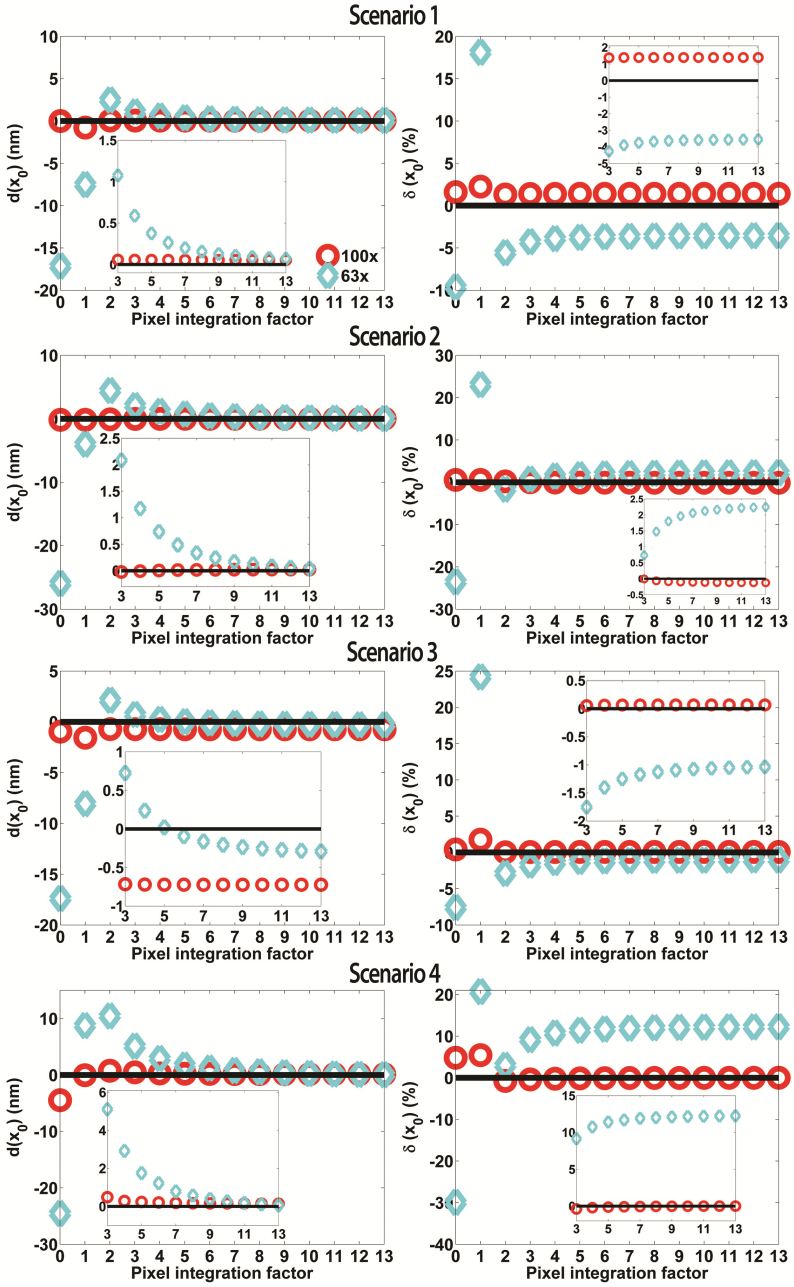

Fig. 3. 2D Gaussian profile results: difference $d(x_0)$ between the median of the x_0 estimates and the true value x_0 (left-hand side plots), and percentage difference $\delta(x_0)$ between the standard deviation (with respect to the median) of the x_0 estimates and the PLAM for x_0 (right-hand side plots), as functions of the PIF used to integrate the image profile during estimation. For each scenario of Table 1, results are shown for a 63× (cyan ⋄) and a 100× (red ○) data set, simulated at PIF = 13 using the 2D Gaussian profile with parameters given in Section 4. Each data set is fitted with a 2D Gaussian profile by an ML estimator, with PIF values ranging from 0 to 13. In all plots the horizontal line denotes 0, and the inset shows the results for PIF ≥ 3.

#237601 Received 6 Apr 2015; revised 18 May 2015; accepted 28 May 2015; published 18 Jun 2015

of d at PIF = 0 and PIF = 13 differ by no more than a quarter of a nanometer in magnitude. In these three cases, the comparable d value is also accompanied by a small percentage difference δ that is comparable to δ at PIF = 13 (difference of less than 0.5% in magnitude in each case), so that the performance of the ML estimator at PIF = 0 is similar to its performance at PIF = 13, despite the simple integration of the image profile.

All in all, our results suggest that the simple integration method for PIF = 0 is more suitable, and hence can be utilized for its faster computational speed, when higher magnifications are used. This can be attributed to the fact that a higher magnification yields a smaller effective pixel size, which produces a finer sampling of the image profile. The finer sampling means that a smaller portion of the image profile is captured by each pixel, and the smaller the portion captured, the better the volume under the profile (i.e., the integral of the profile) over a pixel is approximated by the rectangular volume given by the product of the pixel's area and the profile's value at the center of the pixel.

6.3. Coarser integration of the image profile

We now consider the results for PIF values ranging from 1 to 12, which represent coarser 2D trapezoidal integrations of the image profile than the reference PIF = 13 with which the image data was simulated. For all four scenarios and both the 100× and 63× magnifications, the plots of Figs. 2 and 3 show the difference d to converge to the value of d at PIF = 13 as the PIF is increased from 1 to 12. The convergence points to the importance of integrating at a fine enough step size, especially when the magnification is relatively low. Specifically, in our 63× magnification example, d is large in magnitude at the small PIF values, but decreases quickly towards the value of d at PIF = 13 with increasing PIF. For the 100× magnification, integration step size appears to have a much smaller effect, since the value of d at small PIF values already approaches the value of d at PIF = 13. From the insets, one can clearly see that for PIF = 3 and above, d as a function of the PIF at the 100× magnification is essentially flat relative to d at the 63× magnification.

The plots of Figs. 2 and 3 also show the percentage difference δ to converge to δ at PIF = 13 when the PIF is increased from 1 to 12. As in the case of d, our results suggest that δ is affected by the integration step size to a lesser extent at the 100× magnification. Again from the insets, one can see that for PIF = 3 and above, δ as a function of the PIF at the 100× magnification is relatively constant compared to δ at the 63× magnification.

The difference in the integration step size's degree of impact between the two magnifications can again be attributed to the fineness with which the image profile is sampled. One way of appreciating the difference is that at higher magnifications, the smaller portions of the image profile captured in the pixels encompass smaller variations in the shape of the image profile, and hence allow the value of the integral over each pixel to be relatively well approximated by the use of a coarse integration step size. Therefore, as in the case of PIF = 0, small PIF values are better suited, and can be utilized to improve the computational speed, for integration at higher magnifications.

6.4. Guideline for choosing an appropriate integration step size

The results and analysis of Figs. 2 and 3 demonstrate how the fineness of integration of the image profile over a pixel can impact the performance of the ML estimator for the localization problem. Here we present a method for obtaining a guideline for choosing an appropriate integration step size that ensures estimates that closely recover the true location with an accuracy that is comparable to the PLAM. In the present context, this relates to choosing an appropriate value for the PIF.

We hypothesize that the differences in the performance of the ML estimator at different PIF

#237601 Received 6 Apr 2015; revised 18 May 2015; accepted 28 May 2015; published 18 Jun 2015

values can be attributed to the differences between the image profiles computed using the different PIF values. Therefore, to arrive at a guideline for selecting an appropriate PIF, we quantify the difference between the image profile computed using a given PIF value and the reference image profile, which in the current study is the one computed using the PIF value of 13, as PIF = 13 was used to simulate the image data. More specifically, we calculate a percentage difference by taking the absolute difference between the values of each pair of corresponding pixels in the two image profiles, and dividing the sum of all the absolute differences by the sum of the values of all pixels in the reference image profile. To take into account the positioning of the image profile within the image array, which changes the values of the pixels, we calculate the percentage difference for 121 positions that place the single molecule at regular spacings covering one quadrant of the image array's center pixel, and select the maximum of the 121 percentage differences to be the value that quantifies the difference between the reference image profile and the image profile for the given PIF value. The maximum percentage difference is chosen because it represents the worst case, of all the positions considered, for the given PIF. By looking at the worst case, the guideline that we obtain will be conservative, in the sense that it might specify a PIF value that is higher than necessary. This is preferable, however, to the possibility of underestimating the necessary PIF value.

Note that we consider only positions within the center pixel because it is typical in localization analyses to choose a region of interest that places the image profile in the center. Note also that we sample only one quadrant of the center pixel because the symmetry of the image array allows us to omit the other quadrants. It should also be pointed out we have used 121 positions here to reasonably sample the center pixel quadrant, but one can choose to use a different number of positions.

For the Airy and 2D Gaussian image profiles used in the current study (with parameters given in Section 4), the maximum percentage difference was determined for PIF values of 0 to 13, and for both the 63× and the 100× magnifications. These maximum percentage differences are shown as a function of the PIF in Fig. 4, and apply to all four scenarios of Table 1 because they do not depend on the signal level from the single molecule or the levels of the additive noise sources.

From the figure we see that the curves corresponding to the four combinations of image profile and magnification all look qualitatively similar, and as expected, they show that the image profile becomes more and more similar to the reference image profile (i.e., the maximum percentage difference decreases) as the PIF is increased. From comparison with the $d(x_0)$ and $\delta(x_0)$ curves from the plots of Figs. 2 and 3, these curves also suggest that large percentage differences, which occur at small PIF values, lead to poorer performance by the ML location estimator, and that small percentage differences, which occur at large PIF values, lead to improved performance by the estimator. To obtain a guideline for choosing an appropriate PIF, however, we need a quantitative assessment. For a conservative guideline, we specify the stringent requirement that a given PIF is appropriate only if its corresponding image profile is no more than 1% different from the reference image profile. Applying this guideline, we see a difference between the curves for the two magnifications. For the 63× magnification, a minimum PIF value of 8 is required for both the Airy and the 2D Gaussian profiles. For the 100× magnification, the minimum PIF value is smaller, namely 6 for the Airy profile and 5 for the 2D Gaussian profile. This difference between the magnifications corroborates the finding that the performance of the ML estimator at higher magnifications is impacted to a lesser extent by the use of smaller PIF values.

We find the minimum PIF values based on the 1% guideline to be reasonable. For the 63× magnification, the minimum PIF value of 8 approximately coincides with the point where the difference d and the percentage difference δ begin to level off in the plots of Figs. 2 and 3.

#237601 Received 6 Apr 2015; revised 18 May 2015; accepted 28 May 2015; published 18 Jun 2015

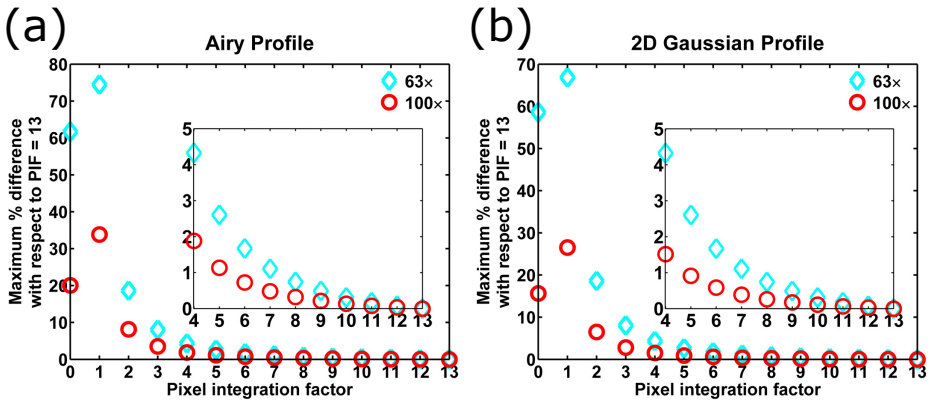

Fig. 4. Obtaining a guideline for determining an appropriate fineness of integration. The maximum percentage difference, as defined in Section 6.4, between the image profile computed using a given PIF value and the reference image profile computed using PIF = 13, is shown as a function of the PIF value for the former for (a) the Airy image profile and (b) the 2D Gaussian image profile. In both (a) and (b), the profiles are computed using the relevant parameters given in Section 4, and the maximum percentage difference is shown for both the 63× (cyan ◇) and the 100× (red ○) magnifications. The inset shows the maximum percentage difference for PIF values ranging from 4 to 13.

The same can be said for the minimum PIF values of 6 and 5 for the Airy and the 2D Gaussian profiles, respectively, for the 100× magnification, and in some cases they lie within the part of the curve that is already essentially level with the value at PIF = 13.

Since the proposed methodology takes into account different positions of the image profile within the center pixel of the region of interest, we should expect the resulting guideline to be applicable regardless of the position of the image profile for a given data set. As a verification, ML estimation was carried out on data sets simulated for the same conditions as for the data sets of Figs. 2 and 3, but with the image profile positioned at 5.5 pixels in both the x and y directions within the 11×11 image array. The results are presented in Figs. 5 and 6, which show that the minimum PIF values of 8 for both image profiles at the 63× magnification, and 6 and 5 for the Airy and 2D Gaussian profiles, respectively, at the 100× magnification, are also reasonable for the localization of the differently positioned single molecule. As is the case for the results presented in Figs. 2 and 3, the results presented in Figs. 5 and 6 are corroborated by the analysis of two additional sets of statistically identical data sets.

Based on the percentage difference between the image profile computed using a given PIF value and the reference image profile, our results suggest that there is indeed a relationship between how well the image profile is evaluated and the performance of the ML localization. The percentage difference clearly depends on the PIF, as different PIF values yield different pixel values for the very same image profile. The percentage difference also depends on the position of the image profile within the image array, however, since the position, as mentioned above, also affects the pixel values. Our analysis of the two different image profile positions, in Figs. 2 and 3 and Figs. 5 and 6, suggests that the PIF affects the magnitude of the percentage difference, and hence the performance of the ML estimator, to a larger extent than the profile position, since for both profile positions considered, small PIF values resulted in worse performance by the estimator, and large PIF values resulted in better performance by the estimator. To demonstrate that the PIF is the main determinant of the estimator's performance, Fig. 7 shows, as a function of the PIF, the mean and standard deviation of the percentage differences for which

#237601 Received 6 Apr 2015; revised 18 May 2015; accepted 28 May 2015; published 18 Jun 2015

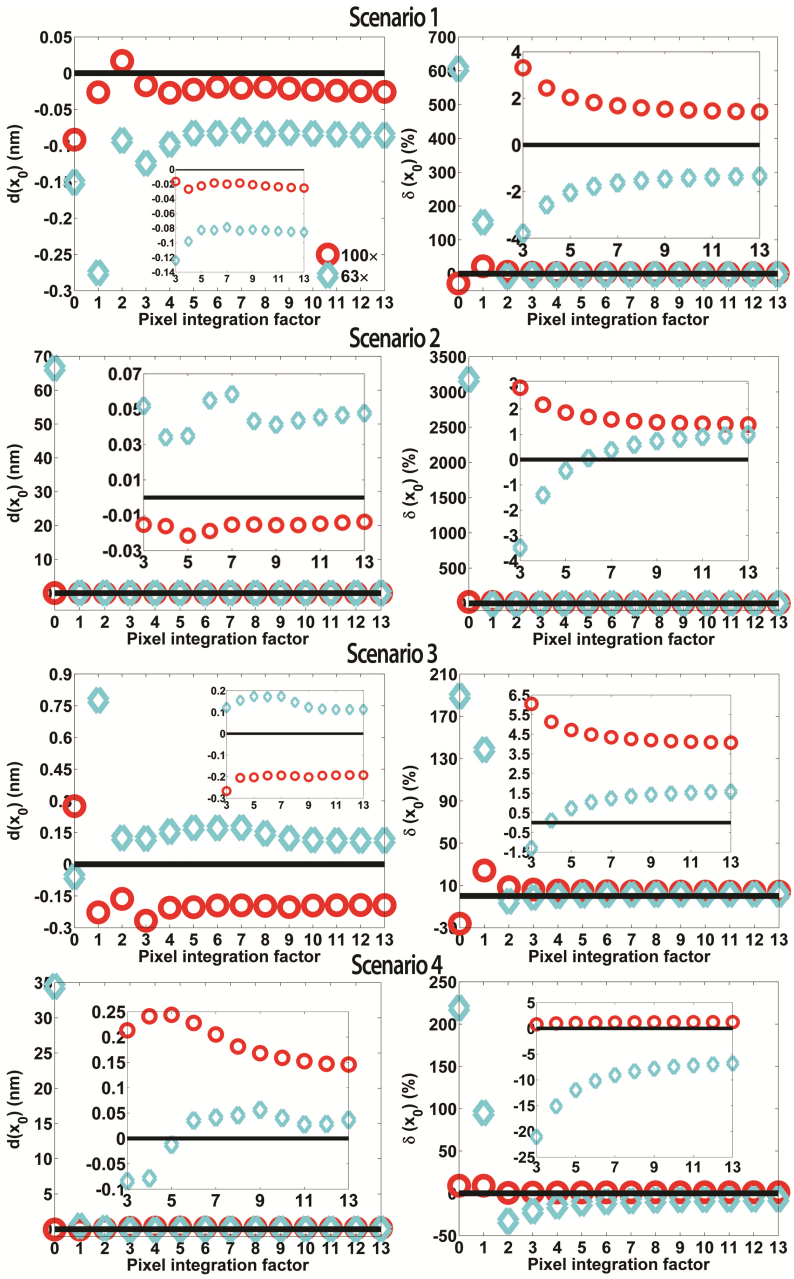

Fig. 5. Airy profile results for a different single molecule location: difference $d(x_0)$ between the median of the x_0 estimates and the true value x_0 (left-hand side plots), and percentage difference $\delta(x_0)$ between the standard deviation (with respect to the median) of the x_0 estimates and the PLAM for x_0 (right-hand side plots), as functions of the PIF used to integrate the image profile during estimation. For each scenario of Table 1, results are shown for a 63× (cyan ⋄) and a 100× (red ○) data set, simulated at PIF = 13 using the Airy profile with parameters given in Section 4, except the molecule is placed at 5.5 pixels in both the x and y directions within the 11×11 image array. Each data set is fitted with an Airy profile by an ML estimator, with PIF values ranging from 0 to 13. In all plots the horizontal line denotes 0, and the inset shows the results for PIF ≥ 3.

#237601 Received 6 Apr 2015; revised 18 May 2015; accepted 28 May 2015; published 18 Jun 2015

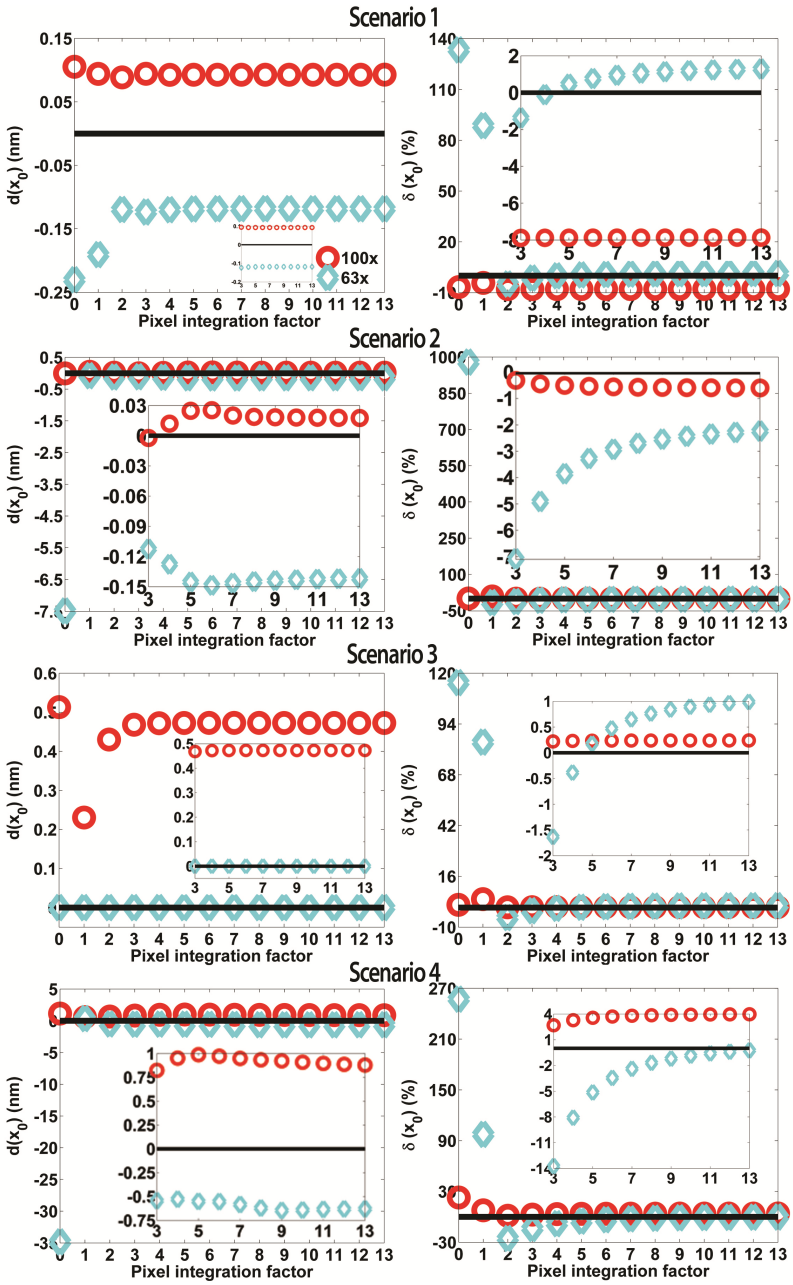

Fig. 6. 2D Gaussian profile results for a different single molecule location: difference $d(x_0)$ between the median of the x_0 estimates and the true value x_0 (left-hand side plots), and percentage difference $\delta(x_0)$ between the standard deviation (with respect to the median) of the x_0 estimates and the PLAM for x_0 (right-hand side plots), as functions of the PIF used to integrate the image profile during estimation. For each scenario of Table 1, results are shown for a 63× (cyan ⋄) and a 100× (red ○) data set, simulated at PIF = 13 using the 2D Gaussian profile with parameters given in Section 4, except the molecule is placed at 5.5 pixels in both the x and y directions within the 11×11 image array. Each data set is fitted with a 2D Gaussian profile by an ML estimator, with PIF values ranging from 0 to 13. In all plots the horizontal line denotes 0, and the inset shows the results for PIF ≥ 3.

#237601 Received 6 Apr 2015; revised 18 May 2015; accepted 28 May 2015; published 18 Jun 2015

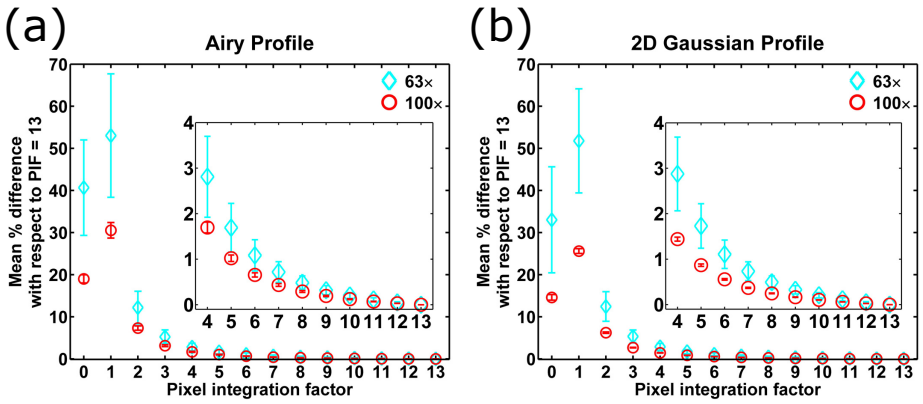

Fig. 7. Mean percentage difference between the image profile computed using a given PIF value and the reference image profile computed using PIF = 13, shown as a function of the PIF value for the former for (a) the Airy image profile and (b) the 2D Gaussian image profile. For each PIF value, the value shown is the mean of the same 121 percentage differences for which the maximum is shown in Fig. 4, and the error bar represents the standard deviation (with respect to the mean) of the 121 percentage differences. In both (a) and (b), the mean percentage difference and the corresponding standard deviation are shown for both the 63× (cyan ⋄) and the 100× (red ○) magnifications. The inset shows the mean percentage difference and the corresponding standard deviation for PIF values ranging from 4 to 13. In (a), the standard deviation as a percentage of the mean, for the 63× magnification, is ∼28% for PIF = 0 and 1, and ∼32% for PIF ≥ 2. For the 100× magnification, it is ∼5% and ∼6% for PIF = 0 and 1, and ∼7% for PIF ≥ 2. In (b), the standard deviation as a percentage of the mean, for the 63× magnification, is ∼38% and ∼24% for PIF = 0 and 1, and ∼28% for PIF ≥ 2. For the 100× magnification, it is ∼5% and ∼2% for PIF = 0 and 1, and ∼3% for PIF ≥ 2.

the maximum is shown in Fig. 4. As can be seen, for all four combinations of image profile and magnification, the mean, as a function of the PIF, exhibits the same pattern as the maximum. Since the mean is representative of the different percentage differences produced by the 121 different positions of the image profile, the preservation of the same pattern indicates that it is the PIF, and not the profile position, that mainly determines the magnitude of the percentage difference, and accordingly the performance of the ML estimator. This is further supported by the relatively small standard deviation of the percentage differences at each PIF value. As shown in Fig. 7, the standard deviations are small enough to suggest that the particular profile position will not substantially alter the relative magnitudes of the percentage differences at the different PIF values.

Figure 7 further demonstrates that if we were to use the mean, rather than the maximum, percentage difference, our guideline would be less conservative, as we would no longer be considering the worst case. The 1% guideline in our current example would become somewhat less conservative, as the plots of Fig. 7 show that the minimum PIF value would decrease to 7 for both image profiles at the 63× magnification, but would remain the same at 6 and 5 for the Airy and 2D Gaussian profiles, respectively, at the 100× magnification.

Note that the proposed methodology is not dependent on the specific numerical integration method or the specific pixel sampling scheme. It can therefore be used to obtain fineness of integration guidelines for numerical integration methods and sampling schemes besides the 2D trapezoidal method and the sampling scheme used in the current study.

#237601 Received 6 Apr 2015; revised 18 May 2015; accepted 28 May 2015; published 18 Jun 2015

7. Conclusions

The computation of image profiles represents an integral task in the analysis of single molecule microscopy data. However, the importance of accurately evaluating the image profile of the single molecule has not been systematically investigated. In this paper, we studied the impact that the fineness with which the image profile is integrated over a pixel has on the performance of the ML location estimator. Our results show that the ability of the estimator to closely recover the true location, and to do so with an accuracy that is comparable to the best possible, is affected by changing the number of points on the pixel at the which the image profile is evaluated for integration. Specifically, we demonstrated that a coarsely integrated image profile can result in substantially poorer performance by the estimator, and that this effect is particularly pronounced at lower magnifications. We also presented a methodology for determining an adequate number of points on the pixel for evaluating the integral of the image profile. The results presented provide useful insight for the optimization of location estimation algorithms, and have implications for applications such as single molecule tracking and superresolution imaging.

Appendix

A.1 Probability distribution of data captured by a pixelated detector

Let $\{z_1,\ldots,z_{K_{pix}}\}$ denote the data acquired by a pixelated detector $\{C_1,\ldots,C_{K_{pix}}\}$. When the data is captured in the presence of additive Poisson and additive Gaussian noise (e.g., scenarios 2 and 4 in Table 1), the probability density function of the data at the kth pixel is given by [1,16]

$$p_{\theta,k}(z_k)=\frac{1}{\sqrt{2\pi}\sigma_{w,k}}\sum_{l=0}^{\infty}\frac{[\nu_{\theta,k}]^l e^{-\nu_{\theta,k}}}{l!}\cdot e^{-\frac{(z_k-l-\eta_k)^2}{2\sigma_{w,k}^2}},\quad z_k\in\mathbb{R},\quad k=1,\ldots,K_{pix},\tag{10}$$

where $\theta\in\Theta$ (Θ denotes the parameter space), η_k and $\sigma_{w,k}$ denote the mean and standard deviation of the additive Gaussian noise at the kth pixel, respectively, and $\nu_{\theta,k}=\mu_{\theta,k}+b_k$, where $\mu_{\theta,k}$ and b_k denote the mean photon counts detected at the kth pixel from the single molecule and the additive Poisson background component, respectively. Note that Eq. (10) also applies when the data is captured in the presence of additive Gaussian noise only, in which case we simply have $b_k=0$, $k=1,\ldots,K_{pix}$. When the data is captured in the presence of additive Poisson noise only, the probability mass function of the data at the kth pixel is given by [1,16]

$$p_{\theta,k}(z_k)=\frac{[\nu_{\theta,k}]^{z_k}e^{-\nu_{\theta,k}}}{z_k!},\quad z_k=0,1,\ldots,\quad k=1,\ldots,K_{pix}.\tag{11}$$

This probability distribution also applies in the absence of any additive noise (e.g., scenarios 1 and 3 in Table 1), in which case we simply have $b_k=0$, $k=1,\ldots,K_{pix}$.

A.2 Noise coefficient

When the data is captured in the presence of additive Poisson and additive Gaussian noise (e.g., scenarios 2 and 4 in Table 1), the noise coefficient for the kth pixel of the detector is given by [1,16,19]

$$\kappa_{\theta,k}=\nu_{\theta,k}\cdot\left[\int_{-\infty}^{\infty}\frac{\left(\frac{1}{\sqrt{2\pi}\sigma_{w,k}}\sum_{l=1}^{\infty}\frac{[\nu_{\theta,k}]^{l-1}e^{-\nu_{\theta,k}}}{(l-1)!}\cdot e^{-\frac{(z-l-\eta_k)^2}{2\sigma_{w,k}^2}}\right)^2}{p_{\theta,k}(z)}dz-1\right],\quad\theta\in\Theta,\tag{12}$$

#237601 Received 6 Apr 2015; revised 18 May 2015; accepted 28 May 2015; published 18 Jun 2015

where $p_{\theta,k}$ is given by Eq. (10). As in the case of Eq. (10), this expression also applies when the data is captured in the presence of additive Gaussian noise only, in which case we simply have $b_k = 0$, $k = 1, \ldots, K_{pix}$. When the data is captured in the presence of additive Poisson noise only, or in the absence of any additive noise (e.g., scenarios 1 and 3 in Table 1), the noise coefficient for the kth pixel is given by [1, 16, 19]

$$\kappa_{\theta,k} = 1, \quad \theta \in \Theta. \tag{13}$$

Acknowledgments

This work was supported in part by the National Institutes of Health (R01 GM085575).

#237601 Received 6 Apr 2015; revised 18 May 2015; accepted 28 May 2015; published 18 Jun 2015